JOURNAL OF PROTEOMICS 84 (2013) 78–91

Available online at www.sciencedirect.com

SciVerse ScienceDirect

www.elsevier.com/locate/jprot

Review

Label-free quantitative proteomic analysis of right ventricular remodeling in infant Tetralogy of Fallot patients

Yu Xia[a,1], Haifa Hong[a,1], Lincai Ye[a], Yanlin Wang[b], Huiwen Chen[a], Jinfen Liu[a,*]

[a]Department of Thoracic and Cardiovascular Surgery, Shanghai Children's Medical Center, Shanghai Jiaotong University School of Medicine, Shanghai, China
[b]Department of Obstetrics, International Peace Maternity and Child Health Hospital, Shanghai Jiaotong University School of Medicine, Shanghai, China

ARTICLE INFO

Article history:
Received 7 November 2012
Accepted 30 March2013
Available online 6 April 2013

Keywords:
Tetralogy of Fallot
Right ventricle
Pressure overload
Hypoxia
Metabolic inflexibility
ECM remodeling

ABSTRACT

Tetralogy of Fallot (TOF) results in chronic progressive right ventricular (RV) pressure overload and shunt hypoxemia. We investigated the global changes in the proteome of RV among infant patients with and without TOF to gain an insight into early RV remodeling. One hundred and thirty-six differentially expressed proteins were identified using label-free LC–ESI-MS/MS analysis. Western blot results revealed that the expression of 6-phosphofructo-2-kinase/fructose-2,6-biphosphatase 2 (PFKFB2) increased significantly in TOF patients; and levels of lysocardiolipin acyltransferase 1 (LCLAT1), lumican (LUM), and versican (VCAN) decreased significantly. QRT-PCR analysis showed that levels of PFKFB2 mRNA were markedly increased, but those of LCLAT1 and LUM were significantly decreased. VCAN mRNA showed no significant change in response to pathophysiology of TOF. The results of immunohistochemical staining were similar to those of Western blot analysis. Results of the proteomic analysis indicated that the level of glycolysis-related proteins had increased and levels of lipid-metabolism-related proteins had decreased. ECM proteins were found to be more down-regulated in TOF in the present study than in previous reports. Taken together, our findings may provide clues to both the metabolic inflexibility and ECM remodeling during the early RV remodeling, which occur in response to chronic hypoxia and long-term pressure overload in TOF patients.

Contents

* *Corresponding author at:* Department of Thoracic and Cardiovascular Surgery, Shanghai Children's Medical Center, Shanghai Jiaotong University School of Medicine, 1678 Dongfang Road, Shanghai 200127, China. Tel.: +86 21 58815377; fax: +86 21 50891405.
E-mail address: liujinfen2013@163.com (J. Liu).
[1] These authors contributed equally to this work and should be considered as co-first author.

1874-3919
http://dx.doi.org/10.1016/j.jprot.2013.03.032

1. Introduction

Congenital heart defects (CHDs), which occur at a rate of approximately 8 per 1000 live births, are the most common life-threatening birth defects [1,2]. Advanced diagnostic and treatment services provided by prenatal screening programs dramatically improve survival and quality of life. This has allowed the number of patients in China with very serious illnesses to increase steadily over the past few decades. Cardiac morphological defects, inducing malhemodynamic overload and shunt hypoxemia, are the two main risk factors for many of these patients. They interfere with the function of the ventricles and cause cardiac hypertrophy and remodeling [3,4].

Tetralogy of Fallot (TOF) is the most common cyanotic complex CHD. The four classic features that characterize TOF are ventricular septal defect (VSD), over-riding of the aorta, right ventricular outflow tract obstruction (RVOTO), and right ventricular hypertrophy [5]. Anatomic defects cause functional abnormalities in TOF patients. Before TOF surgical repair, the main pathophysiological abnormalities are long-term right ventricle (RV) pressure overload and chronic hypoxia. In TOF, significant RVOTO typically includes infundibular hypertrophy and abnormal muscle bundles, which both induce pressure overload, progressive RV hypertrophy, and decreases in pulmonary blood flow. The VSD is almost always large and non-restrictive in TOF. The direction and magnitude of flow through the defect depend on the severity of the RVOTO. If RVOTO is severe, a large right-to-left shunt with low pulmonary blood flow and severe cyanosis are present. However, most patients have adequate pulmonary blood flow at birth but develop increasing cyanosis during the first few weeks or months of life [6]. The treatment of TOF patients requires surgical intervention, and primary repair in the first year of life is the most common strategy [7].

Currently, with the development of surgical strategies for CHD, the pathophysiology of CHD has attracted much more attention, and the importance of RV pathophysiology has also increased. Although there are many published studies addressing RV dysfunction, RV remodeling studies have been limited to the middle and late stages of this condition, and the early stage has been neglected. Exploration of the molecular mechanisms that underlie the pathophysiological changes in early stages among human CHD pediatric patients remains a challenge.

The proteomic approach is a powerful technique used to analyze the complexity of proteins, and elucidate their biological roles, including biochemical processes, structure, and function. Label-free mass spectrometric techniques combined with spectral counting and statistical comparative analysis have yielded data that show considerable reproducibility and utility as a semi-quantitative measure of differential protein abundance [8]. However, proteomic analyses of RV remodeling in human infant TOF are limited.

In the present study, we attempted to study the RV remodeling among infant TOF patients using a label-free quantitative proteomic approach. The purpose was to identify proteins associated with chronic hypoxia, long-term RV pressure overload, and maladaptive processes that occur in response to early cardiac remodeling.

2. Materials and methods

2.1. *Study population*

We recruited 20 CHD patients from the Shanghai Children's Medical Center. The study protocol was approved by the Institutional Research Ethics Committee of Shanghai Children's Medical Center. Informed written consent was obtained from all patients and guardians. Myocardial tissue was collected from the Heart Center of Shanghai Children's Medical Center between November 2011 and March 2012. A total of 10 unrelated patients with sporadic classic TOF were identified, and 10 non-TOF patients lacking deviation of the outlet septum were recruited as controls from among patients undergoing any other type of cardiac surgery (artery valve surgery, coronary artery fistulae). All patients underwent a complete physical examination. Clinical data, including medical records, electrocardiograms, echocardiography, and cardiac

catheterization reports were systematically reviewed. New York University Pediatric Heart Failure Index (NYU PHFI) and modified Ross score were used to evaluate heart function [9]. The RV myocardial tissue specimens were obtained from surgical resection of the right ventricular outflow myocardial tissue to relieve the obstruction. This also confirmed the presence of the TOF phenotype and the absence of any other heart malformation, such as patent ductus arteriosus (PDA) or atrial septal defect (ASD). In general, the fragments of cardiac muscle obtained here were approximately 20 mg in size. The harvested tissue samples were divided into two equal pieces after the bloodstains were removed with normal sterile saline. All samples were frozen in liquid nitrogen immediately after excision and stored at −80 °C.

2.2. Sample preparation

We use filter-aided sample preparation (FASP) to extract protein from the myocardium, as previously described [10]. All samples were analyzed individually and were not pooled at any point. In brief, 10 mg wet tissue was mixed with 200 μl of 8 ml urea in Microcon devices YM-10 (Millipore). The mixtures were centrifuged at 14,000 *g* at 20 °C for 40 min. All the following centrifugation steps were performed using the same conditions. The concentrates were diluted with 200 μl of 8 M urea in 0.1 M Tris–HCl, pH 8.5 and the device was centrifuged. Subsequently, 100 μl of 0.05 M iodoacetamide in 8 M urea in 0.1 M Tris–HCl, pH 8.5 was added to the concentrate and then centrifuged. The resulting concentrate was diluted with 100 μl 8 M urea in 0.1 M Tris–HCl, pH 7.9 and concentrated again. This step was repeated 2 times, and the concentrate was subjected to proteolytic digestion. The products of digestion were collected by centrifugation, and the filter device was rinsed with 50 μl 0.5 M NaCl and centrifuged. The combined filtrates were desalted on an MILI-SPE Extraction disk cartridge; 7 mm per 3 ml (Millipore). The protein concentration was detected by measuring tryptophan fluorescence. Briefly, 1 μl of sample or tryptophan standard (100 ng/μl) was added to 3 ml of 8 M urea buffer (8 M urea, 20 mM Tris–HCl, pH = 7.6). Fluorescence was excited at 295 nm and measured at 350 nm. The slits were set at 10 nm.

2.3. Isoelectric focusing of peptides and mass spectrometric analysis

We separated 0.05 mg of peptides into 12 fractions on the 3100 Offgel Fractionator (Agilent Technologies) as described previously. The immobilized pH gradient strips (IPG strips) from GE Healthcare (Immobiline DryStrip pH 3–10, 13 cm) were rehydrated with 20 μl per well of isoelectric focusing buffer containing 5% glycerol and 50-fold diluted IPG buffer pH 3–10 (GE Healthcare) for 20 min. Peptides were dissolved in 1.68 ml of isoelectric focusing buffer and 0.14 ml of the solution was loaded into to each well. Mineral oil was added to the ends to prevent the filter wicks, which had been wet with buffer, from drying out. Focusing was performed at 20 μA with maximum values of 4500 V, 50 μA, and 200 mW. Focusing was performed for a target of 20 kVh. The focused peptides were acidified using 20 μl of acidic mixture (0.5% acetic acid, 1% TFA and 2% acetonitrile). They were then subjected to desalting and LC–MS/MS analysis. Each sample was analyzed three times by LC–MS/MS.

Protein digestion was analyzed using online high performance liquid chromatography–tandem mass spectrometry (LC–MS/MS). The LC–MS/MS setup was similar to that described in a previous study [11]. Briefly, after the samples were processed in the OFFGEL fractionator, the 12 fractions were clarified to prevent clogging the trapping column with low protein/peptide binding spin filters (0.65 μm pore size) from Millipore. The 12 peptide fractions were infused separately online to a Thermo Electron Finnigan linear ion trap mass spectrometer (LTQ) operated in positive ion mode via a HPLC Agilent 1200 LC system, equipped with a self-packed column (150 μm × 120 mm) at a flow rate of 2 μl/min. The pre-column was washed with mobile phase (95% ACN, 0.1% formic acid) for 20 min to remove any contaminants from the OFFGEL fractionation and the flow was diverted to the separation column (Agilent Zorbax 300SB-C18, 3.5 μm, 75 μm × 150 mm) at a flow rate of 250 nl/min. The peptides were separated and eluted with a linear gradient of 10–60% solution B (0.1% formic acid) in 84 min. Reverse phase-high performance liquid chromatography (RP-HPLC) separation was performed on a Suveyer HPLC system (Thermo Fisher Scientific) equipped with a self-packed column (75 μm × 120 mm) at a flow rate of 250 nl/min. An LTQ-Orbitrap instrument (Thermo Fisher Scientific) was operated in data-dependent mode. The mass spectrometer was set that each full MS scan was followed by 10 most intense ions for MS/MS with charge ≥+2 and the following Dynamic Exclusion™ settings were used: repeat counts, 1; repeat duration, 120 s; exclusion duration, 180 s. The full mass was scanned in Orbitrap analyzer with R = 60,000 (defined at m/z 400), and the subsequent MS/MS analyses were performed in LTQ analyzer.

2.4. Database searching for label-free quantification

All MS/MS spectra were searched using Maxquant software (1.3.0.5) against the human International Protein Index (IPI) database (version 3.87) [12]. Each genuine protein sequence was followed by the reversed amino acid sequence. Two missing cleavage sites were allowed. The tolerances of peptides and fragment ions were set at 6 ppm and 0.5 Da, respectively. The peptide and protein false discovery rate (FDR) was fixed at no more than 0.01. Peptide and protein abundance information were used for label-free quantification as described elsewhere [13].

In our initial studies, we analyzed myocardial proteins of right ventricle tissue from 10 TOF and 10 non-TOF patients. All peptides and proteins identified in this study are listed with posterior error probability values in Table 2.

2.5. Gene ontology analysis

Gene ontology (GO) categories of the identified proteins was performed using the STRAP developed by the Cardiovascular Proteomics Center at the Boston University School of Medicine (http://www.bumc.bu.edu/cardiovascularproteomics/cpctools/strap/) on the basis of Fisher's exact test ($P < 0.01$) [14]. Using a cumulative distribution function-based method, a group of up- and downregulated genes from each data set was statistically tested using the genes' association with each GO entry. We selected the most significant GO terms for each tissue and eliminated redundant GO terms based on the number of genes

that overlapped with other, more significant GO terms. Enriched GO categories under biological process and molecular function were evaluated for differential proteins.

2.6. Immunoblotting

We performed immunoblotting to confirm the results obtained from TOF-MS/MS for four proteins: 6-phosphofructo-2-kinase/fructose-2,6-biphosphatase 2 (PFKFB2), lysocardiolipin acyltransferase 1 (LCLAT1), lumican (LUM), and versican (VCAN). These proteins are representative of glycolysis, metabolism, and extracellular-matrix-related proteins involved in RV remodeling. Blots were processed using commercially available anti-human antibodies: human PFKFB2 polyclonal antibody (AP8146a, Abgent), LCLAT1 polyclonal antibody (AP5723b, Abgent), lumican polyclonal antibody (AP7605a Abgent), versican polyclonal antibody (ab19345 Abcam), and β-actin rabbit monoclonal antibody (4970, Cell Signaling Technology). The secondary antibody used was Dylight 800 labeled affinity antibody to rabbit IgG (072-07-15-06 KPL).

In brief, myocardia were solubilized in Laemmli buffer containing 2-mercaptoethanol. The proteins obtained were separated on 10% SDS polyacrylamide gels. Equal amount of protein (50 μg/lane), estimated using bicinchoninic acid reagent, was loaded. Proteins were then transferred onto nitrocellulose (Immobilon-P Millipore) and the blots were blocked The membranes were blocked with 5% nonfat milk in Tris-buffered saline Tween 20 (TBST) for 2 h at room temperature and then probed with antibodies. Each primary antibody involved in this study was used according to the manufacturer's instructions and diluted to 1:1000–2500. After incubation with corresponding secondary antibodies, the bands were detected using a kit (KPL), diluted to 1:5000, and visualized using an Odyssey infrared imaging system (Odyssey Thera Inc.). Quantitative densitometric image analysis was performed (ImageJ 1.46; http://imagej.nih.gov/ij/). The densitometry of the 45 kDa band was used to normalize the immunoblotting densitometries. Equal loading was confirmed by β-actin immunoblotting.

2.7. Real-time quantitative PCR analysis

The two-step quantitative real-time RT-PCR (QRT-PCR) SYBR Green method (Applied Biosystems) was used to compare and confirm the levels of selected interesting genes. Total RNA was extracted from frozen tissue samples using a RNAsimple Total RNA Kit (Tiangen), as described in the manufacturer's protocol. First-strand cDNA was synthesized using equal amounts of RNA with random primers and PrimeScript RT reverse transcriptase (Takara). The real-time polymerase reaction was conducted using SYBR Green Power Premix (ABI) according to the manufacturer's instructions. The reactions were performed in a total volume of 10 μl and 1.0 μl of cDNA sample was used as a template. An Applied Biosystems 7900 real-time PCR System (ABI) was used as follows: 1 cycle of 10 s at 95 °C followed by 40 cycles of 15 s at 95 °C and 60 s at 60 °C, according to the manufacturer's instructions. The level of mRNA expression was determined with a standard curve and normalized to the mRNA level of 18S ribosomal RNA (18S rRNA). The primer was obtained from Ruijie Bio. (China). The sequences optimized for real-time PCR were as follows: PFKFB2 (sense, 5′-TACGACTTCTTTCGGCATGA; antisense, 3′-CTCCTCTCCCGGGTTGTATT), LCLAT1 (sense, 5′-TGTGGAATT GCCTGATGCGAT; antisense, 3′-TCCAGGAACACCTTTGAGACT), LUM (sense, 5′-CCACCACACCTGACAGAGT; antisense, 3′-CAAG TTGATTGACCTCCAGG), VCAN (sense, 5′-GGTATAGCCCATC TTCCATTTCC and antisense, 3′-TCCTGGTTGGGTCTCCAATTC), and 18S rRNA (sense 5′-GTAACCCGTTGAACCCCATT; antisense, 3′-CCATCCAATCGGTAGTAGCG). All samples were prepared in triplicate to determine their threshold cycle (C_t). Where deviation for each triplicate was higher than 0.3 cycles, C_t was not considered. We show the quantification (n-fold vs. 18S) of three rounds of PCR from at least three independent assays. All samples were run in triplicate with 18S rRNA as an internal control. The sample, control, and target gene were run on the same plate. The fluorescence threshold value was calculated using an ABI Prism Sequence Detection System, version 2.4 (ABI).

2.8. Immunohistochemistry

The specimens were fixed overnight in 4% paraformaldehyde, embedded in paraffin wax, and cut to produce 5 μm-thick sections. For immunohistochemical staining, sections were dewaxed in xylene and rehydrated in serial alcohol. Endogenous peroxidase was blocked by immersing the sections in 0.3% H_2O_2 in methanol for 20 min at room temperature. The specimens were blocked with 3% nonfat milk for 2 h at room temperature and then treated using rabbit polyclonal antibodies against PFKFB2, LCLAT1, LUM, and VCAN at 4 °C for 12–14 h. Anti-PFKFB2 (AP8146a, Abgent), anti-LCLAT1 (AP5723b, Abgent), anti-LUM (AP7605a, Abgent), and anti-VCAN (ab19345 Abcam) were used in accordance with manufacturers' instructions at dilutions of 1:500–1:800. Antigen–antibody complexes were detected using a DAB peroxidase substrate kit according to the manufacturer's protocol (Dako). The negative controls were subjected to the same protocol excepting only that PBS was used instead of the primary antibody. Immunohistochemical staining was semi-quantified using Image Pro Plus 6.0 software on 10 fields of myocardial specimens.

2.9. Statistics

Data were analyzed using the SPSS 17.0 (version 17.0) software package. For clinical data, continuous variables are expressed as mean ± standard deviation (SD) and categorical data are given as numerical values or as percentages. The Student's t or Wilcoxon rank sum tests for continuous variables, the chi-square test for categorical variables, as appropriate. For proteomic analysis, the Student's test was used to compare average ratios between groups. For gene ontology analysis, we corrected values for Bonferroni test. *P*-values below 0.05 were considered statistically significant.

3. Results

3.1. Patients' clinical characteristics

The TOF and non-TOF groups showed no differences in mean height, mean weight, mean age, left ventricular ejection fraction (LVEF), and left ventricular shortening fraction (LVSF)

($P > 0.05$). Oxygen saturation (SO_2) was significantly lower in the TOF group ($P < 0.001$). Peak pulmonary transvalvular gradient ($P < 0.001$), flow rates of main pulmonary artery (MPA, $P < 0.05$), and RV myocardial performance index (Tei index, $P < 0.05$) were significantly higher in the TOF group. The RV hypertrophy was confirmed by echocardiography or cardiac CT. Both the NYU PHFI and modified Ross scores were significantly higher in the TOF group than in the non-TOF group ($P < 0.001$). Cyanosis, tachycardia, tachypnea or dyspnea, hepatomegaly, and failure to thrive were seen among TOF patients. In brief, TOF patients showed early, mild clinically signs of RV dysfunction. Clinical characteristics are shown in Table 1.

3.2. *Identification of 136 differentially expressed proteins by RV myocardium proteomic analysis*

In the proteomic analysis a total of 2030 proteins were identified. Of these, 136 proteins were differentially expressed, showing at least 2.0-fold changes ($P < 0.05$) (Table 2) between two groups. Of these, 53 proteins were up-regulated and 83 proteins were down-regulated.

3.3. *GO analysis of differentially expressed proteins*

Upon gene ontology (GO) analyses of proteins found to be differentially expressed between TOF and non-TOF samples, reasonable representations of biological process and molecular function were obtained. GO analysis showed the most significantly upregulated processes to be in the categories of phosphate transport, response to stimulus, inorganic anion transport, and cell adhesion. Downregulated processes were dominated by energy pathways. The differentially expressed proteins covered 348 biological processes corresponding to cellular process, developmental processes, growth, immune system processes, interaction with cells and organisms, localization, metabolic processes, regulation, reproduction, and response to stimulus. They also covered 188 molecular functions corresponding to antioxidant activity, binding, catalytic activity, enzyme regulator activity, molecular transducer activity, structural molecule activity, and transcription regulator activity. Of these, 88% could be assigned to a known function. 14 proteins could not be assigned to any functions (Table 3) and may be novel proteins involved with RV hypertrophy. The categories and relative occurrence are given in Fig. 1.

3.4. *Immunoblotting*

Western blot analysis was performed to confirm that differentially expressed proteins had been detected by proteomics profiling. We validated the proteomic results using 4 proteins, PFKFB2, LCLAT1, LUM, and VCAN (Fig. 2). These proteins were here considered representative of pathways involved in RV remodeling. β-Actin was used as a loading control. Western blot analysis showed the protein expression of PFKFB2 (TOF/non-TOF ratio 2.43, $P < 0.05$) to be higher in the TOF group and the protein expression of LCLAT1 (TOF/non-TOF ratio 0.32, $P < 0.05$), LUM (TOF/non-TOF ratio 0.47, $P < 0.05$), and VCAN (TOF/non-TOF ratio 0.41, $P < 0.05$) to be lower in the non-TOF group.

3.5. *Real time-PCR*

Changes in the levels of mRNA expression of PFKFB2, LCLAT1, LUM, and VCAN were detected using real-time PCR (Fig. 3). mRNA expression was normalized to the control, 18S rRNA. RT-PCR analysis showed PFKFB2 mRNA expression (TOF/non-TOF ratio 2.23, $P < 0.05$) to be higher in the TOF group than in the non-TOF group and the level of mRNA expression of LCLAT1 (TOF/non-TOF ratio 0.39, $P < 0.05$) and LUM (TOF/non-TOF ratio 0.41, $P < 0.05$) to be lower in the TOF group. The mRNA expression of VCAN (TOF/non-TOF ratio 1.32, $P > 0.05$) showed no significant change between the two groups.

3.6. *Immunohistochemical analysis*

In comparison between non-TOF and TOF by immunohistochemical analysis, protein PFKFB2 (TOF/non-TOF ratio 1.52, $P < 0.05$) was more strongly stained in TOF myocardia than non-TOF myocardia (Fig. 4A, B, C, D, and E), but LCLAT1 protein (TOF/non-TOF ratio 0.63, $P < 0.05$) was more strongly

Table 1 – Clinical information of the patients with and without TOF.

	Non-TOF	TOF	P
Height (cm)	78.70 ± 14.967	69.10 ± 4.533	0.377
Weight (kg)	9.36 ± 3.66	8.25 ± 1.30	0.068
Age (month)	10.90 ± 4.701	9.30 ± 3.164	0.384
Gender (male/female)	4/6	9/1	0.057
Oxygen saturation (SO_2)	98.80 ± 4.442	84.50 ± 6.786	0.001 **
Left ventricular ejection fraction (LVEF)	68.540 ± 5.215	61.170 ± 6.029	0.311
Left ventricular fractional shortening (LVFS)	37.56 ± 4.00	38.450 ± 4.65	0.652
Peak pulmonary transvalvular gradient (mm Hg[a])	25.86 ± 9.67	78.62 ± 16.32	0.000 **
Flow rates of main pulmonary artery (MPA; m/s)	2.26 ± 0.15	4.04 ± 1.37	0.001 *
RV myocardial performance index (Tei index)	0.23 ± 0.02	0.42 ± 0.05	0.012 *
Modified Ross score	2.4 ± 0.84	5.70 ± 0.95	0.000 **
New York University Pediatric Heart Failure Index (NYU PHFI)	5.2 ± 1.69	9.00 ± 2.00	0.000 **

* $P < 0.05$ TOF vs. non-TOF.
** $P < 0.001$ TOF vs. non-TOF.
[a] 1 mm Hg = 0.133 kPa.

Table 2 – Differentially expressed proteins (variations >2.0 fold, $P < 0.05$) in TOF and non-TOF right ventricle tissue specimens.

No.	IPI accession number [a]	Gene symbol	Protein	Seq. cov (%) [c]	TOF spectrum count [b]	Non-TOF spectrum count [b]	Fold change	P-value
1	IPI00022895	A1BG	Alpha-1B-glycoprotein	46.78	33.06 ± 15.75	13.12 ± 5.12	2.52	0.0158
2	IPI00479760	AAK1	AP2-associated protein kinase 1	29.82	69.98 ± 35.76	32.68 ± 3.336	2.14	0.0034
3	IPI00009532	ABAT	4-Aminobutyrate aminotransferase, mitochondrial	39.17	27.93 ± 2.19	164.46 ± 11.98	0.17	0.0256
4	IPI00479296	ABCA8	ATP-binding cassette sub-family A member 8	66.07	15.51 ± 4.92	52.75 ± 3.88	0.29	0.0352
5	IPI00894097	AEBP1	Adipocyte enhancer-binding protein 1	12.30	4.68 ± 1.07	24.64 ± 2.19	0.19	0.0436
6	IPI00016568	AK4	Adenylate kinase isoenzyme 4, mitochondrial	19.78	71.39 ± 14.38	145.84 ± 7.47	0.49	0.0029
7	IPI00940222	AKAP12	A-kinase anchor protein 12	54.93	34.13 ± 3.16	74.47 ± 3.64	0.46	0.0066
8	IPI00965719	ANK2	Ankyrin-2	64.85	12.41 ± 2.46	49.65 ± 5.31	0.25	0.0016
9	IPI00514053	ARCN1	Coatomer subunit delta	20.75	3.10 ± 1.04	31.03 ± 3.87	0.1	0.0401
10	IPI00418431	ASPN	Asporin	48.81	124.12 ± 10.97	319.61 ± 11.71	0.39	0.0107
11	IPI00010790	BGN	Biglycan	69.04	102.40 ± 4.39	335.12 ± 18.92	0.3	0.0453
12	IPI00021727	C4BPA	C4b-binding protein alpha chain	25.39	38.55 ± 4.64	16.26 ± 2.194	2.37	0.0001
13	IPI00022395	C9	Complement component C9	23.86	145.75 ± 32.21	31.82 ± 5.93	4.58	0.0257
14	IPI00843811	C9orf123	Transmembrane protein C9orf123	18.94	46.54 ± 17.32	6.21 ± 1.96	7.5	0.0070
15	IPI00027466	CA4	Carbonic anhydrase 4	26.06	6.21 ± 2.17	43.44 ± 3.93	0.14	0.0150
16	IPI00465436	CAT	Catalase	74.63	192.38 ± 15.36	58.96 ± 7.08	3.26	0.0104
17	IPI00027626	CCT6A	T-complex protein 1 subunit zeta	63.95	80.68 ± 32.18	167.56 ± 8.55	0.48	0.0176
18	IPI00010180	CES1	Liver carboxylesterase 1	23.00	12.41 ± 3.54	52.75 ± 5.28	0.24	0.0324
19	IPI00009028	CLEC3B	Tetranectin	64.24	3.10 ± 1.21	37.24 ± 3.52	0.08	0.0162
20	IPI00024776	CLGN	Calmegin	29.54	31.03 ± 12.86	65.16 ± 3.09	0.48	0.0287
21	IPI00400826	CLU	Clusterin	39.63	12.41 ± 4.32	71.37 ± 5.86	0.17	0.0045
22	IPI00176193	COL14A1	Collagen alpha-1(XIV) chain	62.16	217.21 ± 34.21	471.65 ± 18.55	0.46	0.0131
23	IPI00856012	COL6A6	Collagen alpha-6(VI) chain	54.33	83.78 ± 32.12	226.52 ± 12.16	0.37	0.0085
24	IPI00163230	COPS6	COP9 signalosome complex subunit 6	33.51	15.51 ± 32.34	71.37 ± 3.88	0.22	0.0049
25	IPI00645720	COQ7	Ubiquinone biosynthesis protein COQ7 homolog	23.23	34.13 ± 12.09	102.40 ± 8.78	0.33	0.0023
26	IPI00017601	CP	Ceruloplasmin	35.86	117.91 ± 38.79	245.14 ± 15.51	0.48	0.0072
27	IPI00917030	CPVL	Probable serine carboxypeptidase CPVL	12.36	3.10 ± 0.83	43.44 ± 5.70	0.07	0.0490
28	IPI00031801	CSDA	DNA-binding protein A	28.16	31.03 ± 14.28	3.10 ± 0.98	10.01	0.0036
29	IPI00002824	CSRP2	Cysteine and glycine-rich protein 2	62.92	39.07 ± 8.67	11.25 ± 2.29	3.47	0.0004
30	IPI00012835	CTBP1	C-terminal-binding protein 1	12.98	18.62 ± 5.43	89.99 ± 6.45	0.21	0.0082
31	IPI00010120	CTBP2	C-terminal-binding protein 2	50.33	6.21 ± 2.14	24.82 ± 2.45	0.25	0.0023
32	IPI00019411	CYP2J2	Cytochrome P450 2 J2	50.64	34.13 ± 23.56	3.10 ± 0.96	11	0.0441
33	IPI00028387	DDRGK1	DDRGK domain-containing protein 1	18.73	3.10 ± 1.24	34.13 ± 3.09	0.09	0.0085
34	IPI00024462	DHODH	Dihydroorotate dehydrogenase (quinone), mitochondrial	36.44	46.36 ± 2.45	18.67 ± 5.32	2.48	0.0203
35	IPI00454647	DHRS4-AS1	Putative uncharacterized protein DHRS4-AS1	14.33	18.14 ± 7.63	7.85 ± 2.27	2.31	0.0005
36	IPI00396435	DHX15	Putative pre-mRNA-splicing factor ATP-dependent RNA helicase DHX15	68.99	18.62 ± 9.21	55.85 ± 4.58	0.33	0.0015
37	IPI00465105	DNAJA4	DnaJ homolog subfamily A member 4	34.78	34.13 ± 12.34	3.10 ± 0.92	11.00	0.0109
38	IPI00556073	DNAJB6	DnaJ homolog subfamily B member 6	15.84	71.37 ± 22.98	21.72 ± 2.94	3.28	0.0162
39	IPI00220813	EFEMP1	EGF-containing fibulin-like extracellular matrix protein 1	68.99	9.31 ± 3.01	43.44 ± 3.64	0.21	0.0480
40	IPI00003519	EFTUD2	116 kDa U5 small nuclear ribonucleoprotein component	48.92	18.62 ± 2.90	49.65 ± 2.98	0.38	0.0009
41	IPI00102069	EIF3M	Eukaryotic translation initiation factor 3 subunit M	59.52	37.24 ± 14.32	3.10 ± 1.02	12.00	0.0385
42	IPI00411704	EIF5A	Eukaryotic translation initiation factor 5A-1	52.33	21.72 ± 6.82	93.09 ± 6.03	0.23	0.0079
43	IPI00012510	EMILIN2	EMILIN-2	49.24	102.40 ± 41.05	49.65 ± 3.64	2.06	0.0352
44	IPI00303161	ESAM	Endothelial cell-selective adhesion molecule	13.31	46.54 ± 32.12	6.21 ± 1.96	7.50	0.0183
45	IPI00297550	F13A1	Coagulation factor XIII A chain	25.44	21.72 ± 12.23	58.96 ± 2.71	0.37	0.0316
46	IPI00019568	F2	Prothrombin	46.86	37.24 ± 7.18	105.50 ± 6.735	0.35	0.0345
47	IPI00294615	FBLN5	Fibulin-5	61.22	52.75 ± 20.94	136.53 ± 5.70	0.39	0.0038
48	IPI00298497	FGB	Fibrinogen beta chain	28.04	77.57 ± 25.10	207.90 ± 16.90	0.37	0.0186
49	IPI00021891	FGG	Fibrinogen gamma chain	30.30	127.22 ± 40.18	269.96 ± 12.42	0.47	0.0083

(continued on next page)

Table 2 (*continued*)

No.	IPI accession number [a]	Gene symbol	Protein	Seq. cov (%) [c]	TOF spectrum count [b]	Non-TOF spectrum count [b]	Fold change	P-value
50	IPI00293425	FXN	Frataxin, mitochondrial	66.55	12.41 ± 3.85	49.65 ± 3.65	0.25	0.0053
51	IPI00968027	GC	Vitamin D-binding protein	74.40	37.24 ± 18.3	86.88 ± 15.43	0.43	0.0327
52	IPI00333763	GLRX5	Glutaredoxin-related protein 5, mitochondrial	68.63	24.82 ± 15.43	55.85 ± 3.81	0.44	0.0032
53	IPI00215687	GLS	Glutaminase kidney isoform, mitochondrial	35.01	52.75 ± 13.45	21.72 ± 2.55	2.43	0.0225
54	IPI00894287	HDLBP	High density lipoprotein binding protein	50.33	61.66 ± 13.54	13.85 ± 3.46	4.45	0.0004
55	IPI00003566	HOMER1	Homer protein homolog 1	34.71	3.10 ± 0.24	31.03 ± 3.27	0.1	0.0001
56	IPI00477597	HPR	Haptoglobin-related protein	33.77	6.21 ± 2.40	49.65 ± 5.70	0.13	0.0431
57	IPI00022488	HPX	Hemopexin	23.40	167.56 ± 15.27	341.33 ± 14.62	0.49	0.0057
58	IPI00555565	HSP90AB4P	heat shock protein HSP 90-beta 4	27.21	101.54 ± 36.42	32.75 ± 27.54	3.10	0.0100
59	IPI00217474	IFI16	Gamma-interferon-inducible protein 16	14.87	37.24 ± 9.40	9.31 ± 4.06	4.00	0.0152
60	IPI00018300	IFIT1	Interferon-induced protein with tetratricopeptide repeats 1	44.35	22.99 ± 4.98	8.32 ± 3.68	2.76	0.0100
61	IPI00423461	IGHA2	Ig alpha-2 chain C region	36.08	41.65 ± 15.43	14.29 ± 2.19	2.91	0.0078
62	IPI00896380	IGHM	Ig mu chain C region	49.94	3.10 ± 0.68	62.06 ± 6.72	0.05	0.0124
63	IPI00005198	ILF2	Interleukin enhancer-binding factor 2	52.32	43.44 ± 11.48	117.91 ± 6.51	0.37	0.0385
64	IPI00032328	KNG1	Kininogen-1	21.13	9.31 ± 2.17	52.75 ± 24.63	0.18	0.048
65	IPI00299033	KPNA3	Importin subunit alpha-3	71.77	18.62 ± 3.50	46.54 ± 2.19	0.4	0.0027
66	IPI00012578	KPNA4	Importin subunit alpha-4	72.57	12.41 ± 4.38	43.44 ± 13.93	0.29	0.0287
67	IPI00386803	LASP1	LIM and SH3 domain protein 1	50.55	18.62 ± 4.54	49.65 ± 12.00	0.38	0.0164
68	IPI00419643	LCLAT1	Lysocardiolipin acyltransferase 1	36.82	11.92 ± 2.36	42.05 ± 2.17	0.28	0.0100
69	IPI00009950	LMAN2	Vesicular integral-membrane protein VIP36	35.24	3.10 ± 0.73	24.82 ± 2.85	0.13	0.0361
70	IPI00027847	LPL	Lipoprotein lipase	25.08	6.21 ± 3.67	24.82 ± 12.45	0.25	0.0499
71	IPI00386687	LRRFIP1	Leucine-rich repeat flightless-interacting protein 1	29.71	31.03 ± 2.65	6.21 ± 1.31	5.00	0.0392
72	IPI00020986	LUM	Lumican	27.78	39.09 ± 12.87	81.29 ± 30.11	0.48	0.0038
73	IPI00107722	MCEE	Methylmalonyl-CoA epimerase, mitochondrial	23.11	56.42 ± 16.54	16.34 ± 2.16	3.45	0.0021
74	IPI00022300	METTL7A	Methyltransferase-like protein 7A	73.86	12.41 ± 2.28	52.75 ± 4.64	0.24	0.0116
75	IPI00654820	MT-ATP6	ATP synthase subunit a	73.25	3.10 ± 0.35	27.93 ± 2.29	0.11	0.0085
76	IPI00102685	MYADM	Myeloid-associated differentiation marker	50.27	40.33 ± 7.15	9.31 ± 2.09	4.33	0.0332
77	IPI00790503	MYH10	Myosin-10	58.80	108.60 ± 24.65	217.21 ± 31.92	0.5	0.0407
78	IPI00760846	MYO18A	Myosin-XVIIIa	33.78	52.75 ± 32.65	114.81 ± 7.32	0.46	0.0261
79	IPI00797126	NACA	Nascent polypeptide-associated complex subunit alpha	17.89	148.94 ± 54.71	74.47 ± 5.12	2.00	0.0401
80	IPI00926519	NAGK	N-acetyl-D-glucosamine kinase	41.66	6.21 ± 2.36	24.82 ± 2.19	0.25	0.0401
81	IPI00293817	NAPG	Gamma-soluble NSF attachment protein	44.56	13.67 ± 8.16	3.56 ± 3.09	3.84	0.0145
82	IPI00855737	NEXN	Nexilin	17.66	9.31 ± 3.17	34.13 ± 6.23	0.27	0.0314
83	IPI00465264	NLRX1	NLR family member X1	45.79	40.3413.82	93.09 ± 6.21	0.43	0.0352
84	IPI00299000	PA2G4	Proliferation-associated protein 2G4	75.50	43.44 ± 20.62	9.31 ± 1.50	4.67	0.0229
85	IPI00221111	PACSIN2	Protein kinase C and casein kinase substrate in neurons protein 2	37.28	6.21 ± 1.60	49.65 ± 23.93	0.13	0.0227
86	IPI00980056	PACSIN3	Protein kinase C and casein kinase substrate in neurons protein 3	33.48	15.51 ± 4.29	68.27 ± 15.62	0.23	0.0480
87	IPI00298547	PARK7	Protein DJ-1	63.55	77.57 ± 18.24	24.82 ± 4.09	3.125	0.0120
88	IPI00167134	PDLIM3	PDZ and LIM domain protein 3	60.28	12.41 ± 3.16	89.99 ± 17.52	0.14	0.0134
89	IPI00220808	PFKFB2	6-Phosphofructo-2-kinase/ fructose-2,6-bisphosphatase 2	32.04	34.13 ± 7.82	6.21 ± 1.31	5.5	0.0351
90	IPI00299977	PHPT1	14 kDa phosphohistidine phosphatase	52.58	15.51 ± 5.92	43.44 ± 2.62	0.36	0.0273
91	IPI00216694	PLS3	Plastin-3	46.59	58.96 ± 18.65	145.84 ± 11.71	0.4	0.0055
92	IPI00744711	PNPT1	Polyribonucleotide nucleotidyltransferase 1, mitochondrial	30.99	43.44 ± 32.59	102.40 ± 6.04	0.42	0.0227
93	IPI00165506	POLDIP2	Polymerase delta-interacting protein 2	19.09	108.81 ± 45.36	28.17 ± 2.45	3.86	0.0354
94	IPI00470502	PPA2	Inorganic pyrophosphatase 2, mitochondrial	32.01	74.47 ± 23.43	152.05 ± 6.93	0.49	0.0088
95	IPI00439948	PPP1R13L	RelA-associated inhibitor	41.25	40.33 ± 12.75	9.31 ± 1.53	4.33	0.048
96	IPI00295252	PREX1	Phosphatidylinositol 3,4,5-trisphosphate-dependent Rac exchanger 1 protein	54.17	31.03 ± 14.58	6.21 ± 1.31	5.00	0.0388
97	IPI00305068	PRPF6	Pre-mRNA-processing factor 6	28.27	48.86 ± 17.47	17.94 ± 2.19	2.72	0.0092

Table 2 (*continued*)

No.	IPI accession number [a]	Gene symbol	Protein	Seq. cov (%) [c]	TOF spectrum count [b]	Non-TOF spectrum count [b]	Fold change	P-value
98	IPI00024821	PSMD14	26S proteasome non-ATPase regulatory subunit 14	53.03	27.92 ± 8.22	65.16 ± 4.25	0.43	0.0186
99	IPI00856076	PUF60	Poly(U)-binding-splicing factor PUF60	24.81	40.33 ± 9.78	12.41 ± 3.00	3.25	0.024
100	IPI00016339	RAB5C	Ras-related protein Rab-5C	54.09	40.33 ± 13.64	80.68 ± 4.19	0.5	0.0054
101	IPI00024320	RBM3	Putative RNA-binding protein 3	61.81	28.50 ± 2.78	12.48 ± 4.57	2.28	0.0108
102	IPI00219335	RPL3L	60S ribosomal protein L3-like	61.89	40.34 ± 17.49	12.41 ± 2.17	3.25	0.0073
103	IPI00003918	RPL4	60S ribosomal protein L4	51.06	80.68 ± 29.90	15.51 ± 2.64	5.2	0.0046
104	IPI00221088	RPS9	40S ribosomal protein S9	31.78	89.55 ± 33.43	16.83 ± 2.62	5.32	0.0036
105	IPI00012512	RRAS2	Ras-related protein R-Ras2	56.66	24.82 ± 4.69	3.10 ± 0.97	8.00	0.0072
106	IPI00220558	RYR1	Ryanodine receptor 1	67.02	18.62 ± 4.50	55.85 ± 5.02	0.33	0.0206
107	IPI00329784	RYR3	Ryanodine receptor 3	52.02	46.54 ± 16.07	18.62 ± 2.61	2.50	0.0403
108	IPI00022275	SACM1L	Phosphatidylinositide phosphatase SAC1	74.87	9.31 ± 1.72	37.24 ± 2.85	0.25	0.0197
109	IPI00062266	SCRN2	Secernin-2	74.50	43.44 ± 32.12	9.31 ± 1.50	4.67	0.0375
110	IPI00847635	SERPINA3	Alpha-1-antichymotrypsin	22.67	9.31 ± 1.01	62.06 ± 5.27	0.15	0.0006
111	IPI00027482	SERPINA6	Corticosteroid-binding globulin	13.48	6.21 ± 12.32	24.82 ± 2.45	0.25	0.0041
112	IPI00293074	SLC44A2	Choline transporter-like protein 2	22.29	15.51 ± 4.34	52.75 ± 2.94	0.29	0.0269
113	IPI00893850	SMTN	Smoothelin	71.10	31.03 ± 3.83	9.31 ± 1.48	3.33	0.0215
114	IPI00299095	SNX2	Sorting nexin-2	73.03	9.31 ± 6.94	34.13 ± 2.75	0.27	0.0453
115	IPI00291419	SOAT2	Sterol O-acyltransferase 2	25.50	3.10 ± 0.35	27.93 ± 3.05	0.11	0.0261
116	IPI00027827	SOD3	Extracellular superoxide dismutase [Cu–Zn]	35.07	55.85 ± 13.88	111.71 ± 35.51	0.5	0.0287
117	IPI00103415	STAT5B	Signal transducer and activator of transcription 5B	47.16	3.10 ± 31.85	27.93 ± 3.06	0.11	0.0352
118	IPI00019903	TACO1	Translational activator of cytochrome c oxidase 1	29.40	37.24 ± 11.85	96.19 ± 5.52	0.39	0.0344
119	IPI00386607	TBCD	Tubulin-specific chaperone D	41.48	83.05 ± 34.85	35.12 ± 3.09	2.36	0.0130
120	IPI00160479	TECRL	Trans-2,3-enoyl-CoA reductase-like	56.55	6.21 ± 2.84	37.24 ± 8.07	0.17	0.0458
121	IPI00385317	TENC1	Tensin-like C1 domain-containing phosphatase	44.02	28.80 ± 10.35	10.96 ± 2.64	2.63	0.0209
122	IPI00022462	TFRC	Transferrin receptor protein 1	57.83	161.36 ± 57.98	68.27 ± 4.09	2.36	0.0261
123	IPI00794391	THSD4	Thrombospondin type-1 domain-containing protein 4	45.66	6.21 ± 2.32	37.24 ± 3.81	0.17	0.0147
124	IPI00001541	TIMM9	Mitochondrial import inner membrane translocase subunit Tim9	12.09	3.10 ± 0.53	21.72 ± 2.56	0.14	0.0199
125	IPI00063130	TMEM205	Transmembrane protein 205	37.26	21.72 ± 9.38	46.54 ± 2.19	0.47	0.0499
126	IPI00005087	TMOD3	Tropomodulin-3	43.50	149.04 ± 48.23	73.02 ± 2.29	2.04	0.0383
127	IPI00100247	TMX4	Thioredoxin-related transmembrane protein 4	37.78	159.74 ± 33.85	37.90 ± 3.57	4.21	0.0052
128	IPI00939667	TPP1	Tripeptidyl-peptidase 1	34.68	74.47 ± 3.56	148.94 ± 35.63	0.50	0.0344
129	IPI00301561	TRIP6	Thyroid receptor-interacting protein 6	44.04	27.93 ± 3.43	3.10 ± 0.89	9.00	0.0199
130	IPI00292858	TYMP	Thymidine phosphorylase	40	21.11 ± 11.26	7.29 ± 4.57	2.89	0.0397
131	IPI00830039	U2AF2	Splicing factor U2AF 65 kDa subunit	18	15.51 ± 9.34	40.34 ± 2.65	0.38	0.0480
132	IPI00003965	USP7	Ubiquitin carboxyl-terminal hydrolase 7	30	27.96 ± 16.28	9.16 ± 2.19	3.05	0.0200
133	IPI00215631	VCAN	Versican core protein	72	71.37 ± 36.73	170.66 ± 8.56	0.42	0.0034
134	IPI00032050	WBP2	WW domain-binding protein 2	14	34.13 ± 8.73	3.10 ± 0.99	10.00	0.0131
135	IPI00922067	XPNPEP3	Probable Xaa-Pro aminopeptidase 3	15	3.10 ± 1.58	31.03 ± 2.94	0.10	0.0230
136	IPI00166738	ZADH2	Zinc-binding alcohol dehydrogenase domain-containing protein 2	30	34.13 ± 5.07	3.10 ± 0.87	11.00	0.0333

[a] Accession number from EMBL-EBI (International Protein Index, IPI).
[b] Scores based on the average of each sample's spectral counting.
[c] Percentage of sequence coverage.

stained in non-TOF myocardia than in TOF myocardia (Fig. 4F, G, H, I, and J). LUM protein (TOF/non-TOF ratio 0.59, $P < 0.05$) was more strongly stained in TOF extracellular regions than in non-TOF extracellular regions (Fig. 4K, L, M, N, and O). Levels of VCAN protein (TOF/non-TOF ratio 0.68, $P < 0.05$) were clearly higher in TOF extracellular regions (Fig. 4P, Q, R, S, and T) than in non-TOF extracellular regions. Semi-quantification graphs are shown (Fig. 4E, J, O, and T; *, $P < 0.05$).

4. Discussion

Our study profiled differential protein expression during RV remodeling in developing hearts with congenital malformation. We speculated that maladaptive response to long-term pressure overload and chronic hypoxia could be the immediate causes of the RV remodeling. Some of the differentially

Table 3 – 14 proteins not assigned to any functions. [a]

Gene symbol	Location	Tissue specificity	Biology process	Cellular component	Molecular function
A1BG	19q13.4	Plasma	\	Extracellular region	\
C9orf123	9p24.1	\	\	Integral to membrane [d]	\
DDRGK1	20p13	Ubiquitously expressed (at protein level)	\	Endoplasmic reticulum	\
DHRS4-AS1	14q11.2	\	\	\	\
DNAJA4	15q25.1	\	Protein folding/response to heat [d]	Membrane [d]	ATP binding [d]/metal ion binding [d]
HPR	16q22.1	\	Metabolic process [d]	Spherical high-density lipoprotein particle	Catalytic activity [d]
MYADM	19q13.42	Widely expressed. Not detected in thymus	\	Integral to membrane	\
POLDIP2	17q11.2	\	\	Mitochondrial nucleoid/ nucleus [d]	DNA binding [d]
PPA2	4q25	Detected in brain, gastric carcinoma, lung, ovary, skeletal muscle, umbilical cord blood and a cell line derived from kidney proximal tubule epithelium	Diphosphate metabolic process [b]/phosphate-containing compound metabolic process [d]/tRNA aminoacylation for protein translation [b]	Mitochondrial matrix [b]	Inorganic diphosphatase activity [b] /magnesium ion binding [d]
SCRN2	17q21.32	\	Proteolysis [d]	Dipeptidase activity [d]	\
TECRL	4q13.1	\	Lipid metabolic process [d]	Cytoplasm/integral to membrane [d]	Oxidoreductase activity, acting on the CH–CH group of donors [d]
TMX4	20p12	\	Cell redox homeostasis [d]/ electron transport chain [d]	Integral to membrane	\
WBP2	17q25	Ubiquitous	\	\	\
ZADH2	18q22.3	\	Mitochondrion [d]/ peroxisome [c]	Nucleotide binding [d]/ oxidoreductase activity [d]/ zinc ion binding [d]	\

[a] Information from UniProt.
[b] Traceable author statement.
[c] Inferred from sequence or structural similarity.
[d] Inferred from electronic annotation.

expressed proteins were found to play important roles in certain biological processes related to cardiac remodeling, including the regulation of glycolysis, oxidation and reduction, oxidative stress, metabolism, cell death, ion homeostasis, and protein transport. They showed that RV was affected by pressure overload and chronic hypoxia in infants with TOF. We further confirmed the expression of metabolic enzymes, such as 6-phosphofructo-2-kinase/fructose-2,6-bisphosphatase 2 (PFKFB2) and lysocardiolipin acyltransferase 1 (LCLAT1).

PFKFB2 is mainly expressed in the heart, brain, and lungs. It belongs to the 6-phosphofructo-2-kinase/fructose-2,6-bisphosphatase (PFKFB) family [15]. PFKFB2 is the most potent allosteric activator of phosphofructokinase (PFK-1), which is a key regulator of glycolytic flux. Cellular levels of PFKFB2 are correlated to the intensity of glycolytic flux. In this way, the cardiac PFKFB2 isoform is essential to the regulation of glycolysis in the heart [16]. Minchenko showed that hypoxia was associated with a slight downregulation of PFKFB2 mRNA expression in the hearts of affected mice [17]. Unlike Minchenko, we discovered that protein and mRNA levels of PFKFB2 were significantly higher in TOF patients than in unaffected individuals. We speculated that methodological differences may account for this discrepancy. Specifically, the mice used in the Minchenko's study were kept in hypoxic environments for only 6 h, but in our study, pathophysiological hypoxia and malhemodynamics of TOF lasted for at least 8 months. PFKFB2 was also found to be highly expressed in tissues undergoing tumorigenesis, which preferentially use glycolysis to meet the tumors' increased energetic and biosynthetic requirements (Warburg effect) [18]. Like tumors, under pathological stress conditions, cardiomyocytes gradually come to rely on glycolysis to meet their main energy requirements. This is called cardiac metabolic inflexibility [19,20]. We also identified other proteins related to glycolysis, such as PFK-1 and HK (hexokinase), and found that they have an upward trend in TOF. However, the levels of these proteins did not show significant differences (data not shown).

Lysocardiolipin acyltransferase 1 (LCLAT1) was recently shown to catalyze pathological remodeling of CL in response to oxidative stress in individuals with diabetes, obesity, and cardiomyopathy, leading to ROS production, mitochondrial dysfunction, and insulin resistance [21–23]. CL pathological remodeling by ALCAT1 overexpression leads to the synthesis of CL with aberrant acyl composition. It has been implicated in the etiology of mitochondrial dysfunction, including depletion of linoleic acid and enrichment of DHA content in CL. Ablation of ALCAT1 has been shown to mitigate oxidative stress and prevent mitochondrial dysfunction by up-regulating levels of

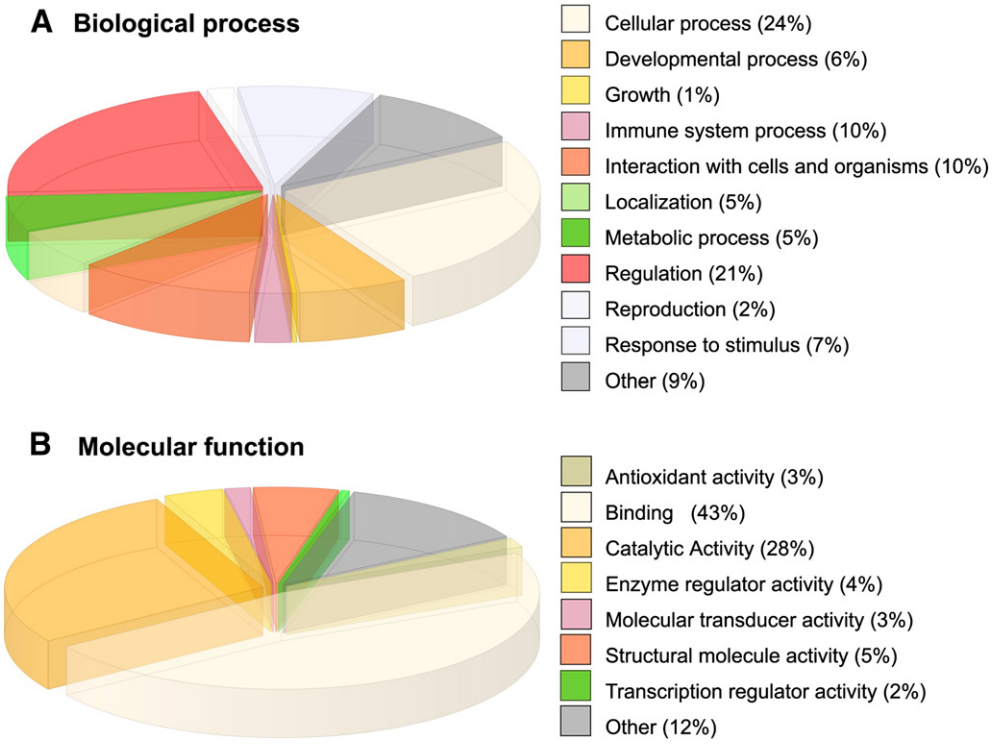

Fig. 1 – The identified proteins were classified based on known biological process (A) and molecular function (B).

PINK1, which is required for mitochondrial autophagy, and of MFN2 [24,25]. Cao found ALCAT1 expression in liver and heart to be significantly downregulated in mice with hypothyroidism and upregulated in mice treated with thyroid hormone, suggesting that changes in LCLAT1 expression can meet the need for cardiolipin remodeling in response to changes in mitochondrial activity and ROS levels [23]. Conversely, we found that the level of expression of protein and mRNA LCLAT1 decreased in the TOF group. We also found SOD3 level decreased in TOF group. Eva Nozik-Grayck, found that chronic hypoxic decreased SOD activity and protein expression, suggesting that hypoxic adaptation did not impaired mitochondria and ROS level was low [26]. Moreover, cumulative evidence suggests that LCLAT1 didn't relate to pressure overload increase [27–29]. Our data suggested that LCLAT1 expression may become significantly downregulated during chronic hypoxia, which decreases levels of oxidative stress and ROS production.

In normal hearts, fatty acid is the main energy resource. Loss of metabolic flexibility such as, substantial metabolic switch from fatty acid oxidation to glycolysis, would be potentially harmful to heart function [30]. In this extended study, we observed somewhat similar qualitative changes and elevations in the levels of proteins related to glycolysis. No

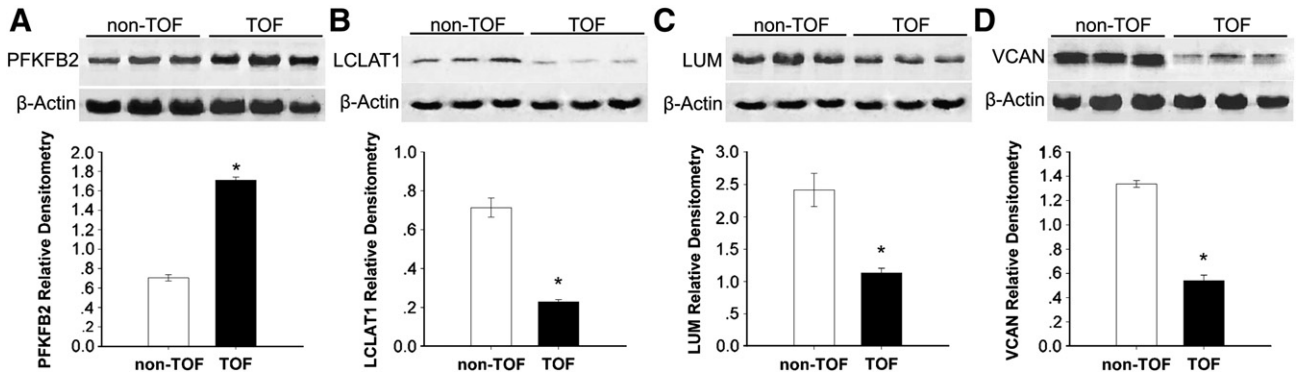

Fig. 2 – Western blot analysis of the levels of proteins in myocardial tissues. Western blots to detect PFKFB2 (A), LCLAT1 (B), LUM (C) and VCAN (D) in non-TOF (left panel) and TOF (right panel). Equal amounts of total protein were loaded (50 μg). A representative graph is shown along with the numeric data obtained by densitometry analysis (below each panel). β-Actin served as loading control. The bars indicate mean ± SD. Student's test was performed to evaluate statistical significance. (*, $P < 0.05$, n = 3).

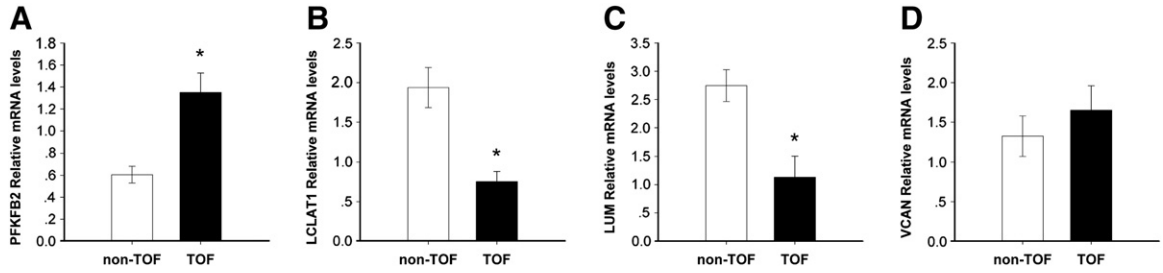

Fig. 3 – The mRNA expression level of PFKFB2 (A), LCLAT1 (B), LUM (C) and VCAN (D) was further verified by real time-PCR. The distribution of PFKFB2 was increased ($P < 0.05$), LCLAT1 and LUM decreased respectively ($P < 0.05$). VCAN does not show significant changes between two groups ($P > 0.05$). The bars indicate mean ± SD. Student's test was performed to evaluate statistical significance. (*, $P < 0.05$).

specific proteins were found to be directly associated with fatty acid oxidation in our experiment. However, we noted a substantial decline in lipid metabolic processes relative to fatty acid oxidation in TOF. For example, CYP2J2 (fatty acid biosynthetic process), clusterin, high-density lipoprotein binding protein (lipid transport), lipoprotein lipase (triglyceride catabolic process), soat2 (lipid modification), and LCLAT1 (lipid biosynthetic process) [31–35]. It can be concluded that the overall rate of general lipid metabolic processes decreases in response to pathophysiological changes in TOF. This metabolic change decreases cardiac efficiency and energetic utilization. Specifically, metabolic inflexibility may be detrimental to heart function during early phases due to maladaptive responses.

The extracellular matrix (ECM) protein lumican (LUM) belongs to a family of small leucine-rich proteoglycans (SLRPs). Previous studies have shown that LUM contributes mainly to collagen fiber assembly and organization in fibrotic lesions in ischemic and reperfused hearts [36]. LUM may be related to heart failure irrespective of age and sex [37]. Waehre observed an elevation in total levels of LUM protein in the pressure-overloaded RV tissue of the mice 7 days after pulmonary artery banding (PAB) [38]. We found LUM protein and mRNA to be more abundant in non-TOF samples than in TOF samples. This was consistent with Hwang's earlier findings showing decreased LUM mRNA expression in end-stage heart failure with hypertrophic cardiomyopathy (HCM). Sharing pathophysiological similarity with TOF, HCM patients showed dyspnea, heart ventricle hypertrophy, and RVOTO [39]. Some recent studies have shown that LUM can stop endothelial cells from activating p38 MAPK and prevent invasion, angiogenic sprouting, and vessel formation [40]. Many studies have confirmed that angiogenesis can provide potential compensative benefits for heart failure. Hypertrophy overload can also cause angiogenic and metabolic genes to meet the greater demand for nutrients. In this way, angiogenic factors can act as novel therapeutic targets [41]. These data suggest that the pattern of LUM expression is different under hypertrophic and hypoxic conditions but closely associated with the pathology of tissue repair. Low levels of LUM expression could contribute to anti-myocardial fibrosis and angiogenesis in TOF pathology.

Versican (VCAN) is a large chondroitin sulfate proteoglycan, specialized in mediating cell proliferation, adhesion, and migration. A wide distribution of VCAN was found in various organs, including the heart. Its contribution to the pathological conditions of the vessels such as atherosclerosis and vascular injury has also been established [42]. Hellman observed the up-regulation of VCAN at day 1, and this elevated level of VCAN later subsided to control levels, as recorded on days 6 and 42 [43]. Kern found that G1-containing VCAN and intact VCAN reduced myocardial cell–cell association and that VCAN proteolysis mediates loss of the distal myocardium during outflow tract development [44]. These results suggested that a high level of VCAN protein may exhibit an opposing effect on myocardial cells during cardiac remodeling. Like LUM, we found a decreased level of VCAN protein and mRNA in TOF. However, it remains unclear for us about the relationship between hypoxia and expression of VCAN. Further studies should be proposed to unveil the potential pathophysiologic implications of the decreased VCAN in TOF.

We compared our results to those of previous, analogous studies [45–52]. The protein profile showed a distinct pattern, and small parts of this pattern overlapped with the results of those reports. We found human CHD to differ from the traditional pulmonary artery banding animal model in its pathophysiological process, time to progression, and molecular basis. Age, treatment, and other complications were found to affect the proteomic profile. The heterogeneity of subjects could explain why previous studies had different findings.

In addition, we also found that some unknown function genes have potential in relation to cardiac hypertrophy, such as Dnaja4 which plays a role in the development of coronary microvascular remodeling in spontaneously hypertensive rat (SHR) [53].

In conclusion, powerful comparative label-free proteomic techniques were used to show the differential proteomic profile during RV remodeling in CHD with chronic hypoxia and long-term pressure overload. Results of the proteomic analysis also indicated that the level of proteins related to glycolysis increased and the level of proteins related to lipid metabolism decreased. The ECM proteins showed a down-regulated change under pathophysiological TOF conditions, and this change was not detected in previous reports. These findings indicate that TOF is a suitable model for the study of RV pressure overload and hypoxia during cardiac remodeling and that it may provide information on the metabolic inflexibility and ECM remodeling that take place during the early stages of RV remodeling in TOF. It may open new means

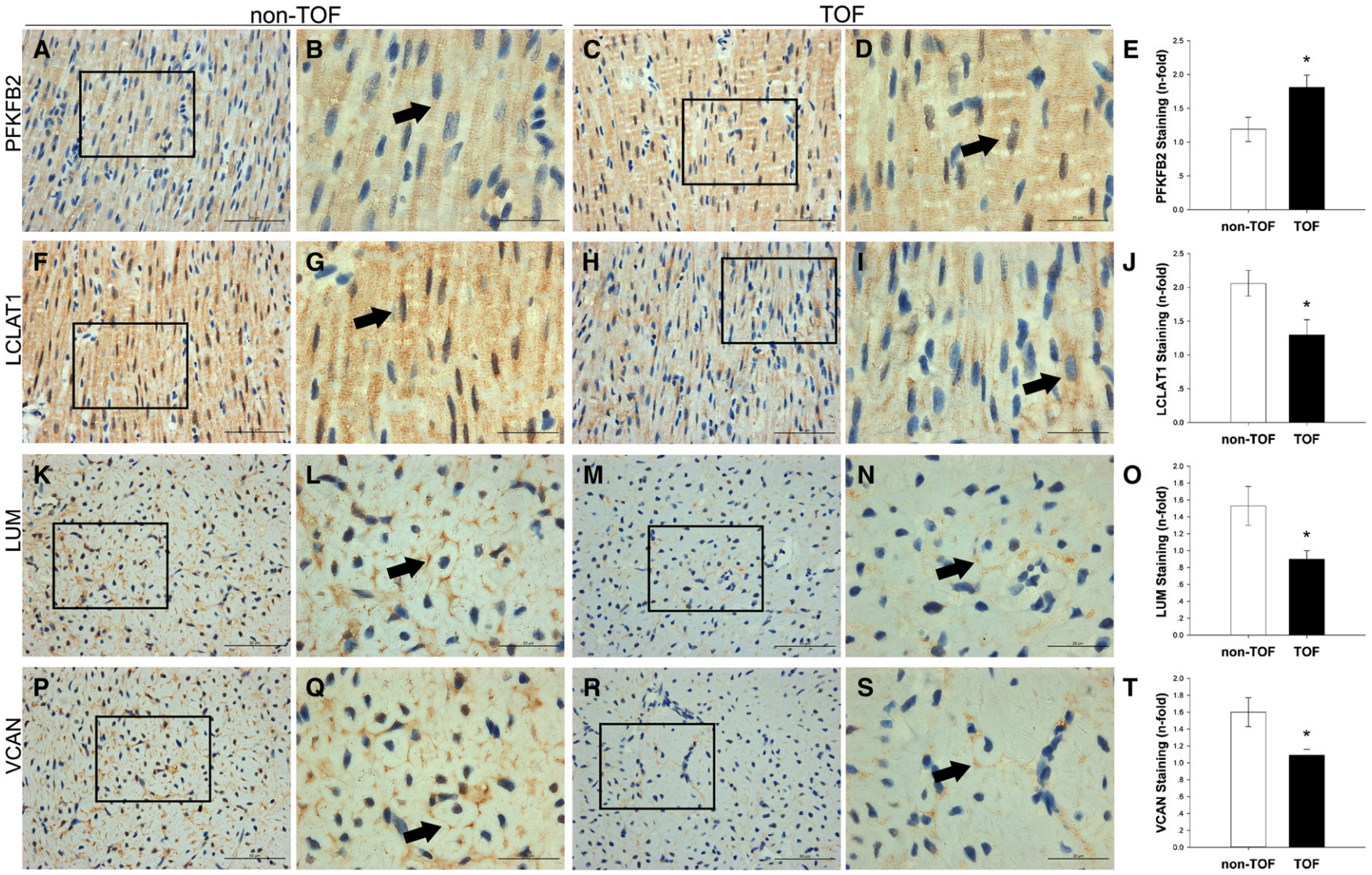

Fig. 4 – Representative immunohistochemical staining of PFKFB2, LCLAT1, LUM and VCAN in RV tissues from non-TOF (A, B, F, G, K, L, P, and Q), and TOF (C, D, H, I, M, N, R, and S). The tissue sections were dewaxed in xylene and rehydrated in graded alcohols. After unmasking antigen and removing endogenous peroxidases, sections were incubated for 12–14 h with antibodies against PFKFB2 (A, B, C, and D), LCLAT 1 (F, G, H, and I), LUM (K, L, M, and N) and VCAN (P, Q, R, and S), respectively, and detected with HRP-conjugated secondary antibody and DAB substrate chromogen solution. Immunohistochemical analysis revealed that PFKFB2 and LCLAT1 were mainly expressed in the cytoplasm of the myocardium (B, D, G, and I), LUM and VCAN were mainly expressed in the extracellular region (L, N, Q, and S). A, C, F, H, K, M, P, and R magnification ×40, scale bars: 50 μm; B, D, J, I, L, N, Q, and S magnification ×100, scale bars: 20 μm. Note that the stained patterns (E, G, O, and T) were correlated with Western blotting data.

of understanding cardiac maladaptation. Further studies are needed to analyze the proteomics of specific cell populations, to identify the changes in the levels of less abundant proteins, and to determine the effects of post-translational modifications (PTM).

Acknowledgments

The authors have no financial conflicts of interest to declare. This work was supported by the major project of the Shanghai Committee of Science and Technology, China (grant no. 10DZ1951200), National Basic Research Program of China (973 Program-2013CB945304) and by a grant from the National Natural Science Foundation of China (no. 81200128). We would like to thank Qingjian Chen of the University of Maryland, College Park for the help during the preparation of this manuscript.

REFERENCES

[1] Roger VL, Go AS, Lloyd-Jones DM, Benjamin EJ, Berry JD, Borden WB, et al. Heart disease and stroke statistics—2012 update: a report from the American Heart Association. Circulation 2012;125:e2-220.
[2] Bernier PL, Stefanescu A, Samoukovic G, Tchervenkov CI. The challenge of congenital heart disease worldwide: epidemiologic and demographic facts. Semin Thorac Cardiovasc Surg Pediatr Card Surg Annu 2010;13:26–34.
[3] Del Duca D, Tadevosyan A, Karbassi F, Akhavein F, Vaniotis G, Rodaros D, et al. Hypoxia in early life is associated with lasting changes in left ventricular structure and function at maturity in the rat. Int J Cardiol 2012;156:165–73.
[4] Minegishi S, Kitahori K, Murakami A, Ono M. Mechanism of pressure-overload right ventricular hypertrophy in infant rabbits. Int Heart J 2011;52:56–60.
[5] Anderson RH, Jacobs ML. The anatomy of Tetralogy of Fallot with pulmonary stenosis. Cardiol Young 2008;18:12–21.
[6] Anderson RH, Weinberg PM. The clinical anatomy of Tetralogy of Fallot. Cardiol Young 2005;15:38–47.
[7] Al Habib HF, Jacobs JP, Mavroudis C, Tchervenkov CI, O'Brien SM, Mohammadi S, et al. Contemporary patterns of management of Tetralogy of Fallot: data from the Society of Thoracic Surgeons Database. Ann Thorac Surg 2010;90:813–20.
[8] Dicker L, Lin X, Ivanov AR. Increased power for the analysis of label-free LC–MS/MS proteomics data by combining spectral counts and peptide peak attributes. Mol Cell Proteomics 2010;9:2704–18.
[9] Connolly D, Rutkowski M, Auslender M, Artman M. The New York University Pediatric Heart Failure Index: a new method of quantifying chronic heart failure severity in children. J Pediatr 2001;138:644–8.
[10] Wiśniewski JR, Zougman A, Nagaraj N, Mann M. Universal sample preparation method for proteome analysis. Nat Methods 2009;6:359–62.
[11] Warren CM, Geenen DL, Helseth Jr DL, Xu H, Solaro RJ. Sub-proteomic fractionation, iTRAQ, and OFFGEL-LC–MS/MS approaches to cardiac proteomics. J Proteomics 2010;73:1551–61.
[12] Cox J, Mann M. MaxQuant enables high peptide identification rates, individualized p.p.b.-range mass accuracies and proteome-wide protein quantification. Nat Biotechnol 2008;26:1367–72.
[13] Luber CA, Cox J, Lauterbach H, Fancke B, Selbach M, Tschopp J, et al. Quantitative proteomics reveals subset-specific viral recognition in dendritic cells. Immunity 2010;32:279–89.
[14] Bhatia VN, Perlman DH, Costello CE, McComb ME. Software tool for researching annotations of proteins: open-source protein annotation software with data visualization. Anal Chem 2009;81:9819–23.
[15] van Lunteren E, Spiegler S, Moyer M. Contrast between cardiac left ventricle and diaphragm muscle in expression of genes involved in carbohydrate and lipid metabolism. Respir Physiol Neurobiol 2008;161:41–53.
[16] Arden C, Hampson LJ, Huang GC, Shaw JA, Aldibbiat A, Holliman G, et al. A role for PFK-2/FBPase-2, as distinct from fructose 2,6-bisphosphate, in regulation of insulin secretion in pancreatic beta-cells. Biochem J 2008;411:41–51.
[17] Minchenko O, Opentanova I, Caro J. Hypoxic regulation of the 6-phosphofructo-2-kinase/fructose-2,6-bisphosphatase gene family (PFKFB-1-4) expression in vivo. FEBS Lett 2003;554:264–70.
[18] Vriens MR, Moses W, Weng J, Peng M, Griffin A, Bleyer A, et al. Clinical and molecular features of papillary thyroid cancer in adolescents and young adults. Cancer 2011;117:259–67.
[19] Wang Q, Donthi RV, Wang J, Lange AJ, Watson LJ, Jones SP, et al. Cardiac phosphatase-deficient 6-phosphofructo-2-kinase/fructose-2,6-bisphosphatase increases glycolysis, hypertrophy, and myocyte resistance to hypoxia. Am J Physiol Heart Circ Physiol 2008;294:H2889–97.
[20] Oka T, Lam VH, Zhang L, Keung W, Cadete VJ, Samokhvalov V, et al. Cardiac hypertrophy in the newborn delays the maturation of fatty acid beta-oxidation and compromises postischemic functional recovery. Am J Physiol Heart Circ Physiol 2012;302:H1784–94.
[21] Wang W, Ni L, Yu Q, Xiong J, Liu HC, Rosenwaks Z. Expression of the Lycat gene in the mouse cardiovascular and female reproductive systems. Dev Dyn 2010;239:1827–37.
[22] Li J, Romestaing C, Han X, Li Y, Hao X, Wu Y, et al. Cardiolipin remodeling by ALCAT1 links oxidative stress and mitochondrial dysfunction to obesity. Cell Metab 2010;12:154–65.
[23] Cao J, Shen W, Chang Z, Shi Y. ALCAT1 is a polyglycerophospholipid acyltransferase potently regulated by adenine nucleotide and thyroid status. Am J Physiol Endocrinol Metab 2009;296:E647–53.
[24] Liu X, Ye B, Miller S, Yuan H, Zhang H, Tian L, et al. Ablation of ALCAT1 mitigates hypertrophic cardiomyopathy through effects on oxidative stress and mitophagy. Mol Cell Biol 2012;32:4493–504.
[25] Li J, Liu X, Wang H, Zhang W, Chan DC, Shi Y. Lysocardiolipin acyltransferase 1 (ALCAT1) controls mitochondrial DNA fidelity and biogenesis through modulation of MFN2 expression. Proc Natl Acad Sci U S A 2012;109:6975–80.
[26] Nozik-Grayck E, Suliman HB, Majka S, Albietz J, Van Rheen Z, Roush K, et al. Lung EC-SOD overexpression attenuates hypoxic induction of Egr-1 and chronic hypoxic pulmonary vascular remodeling. Am J Physiol Lung Cell Mol Physiol 2008;295:422–30.
[27] Mrnka L, Nováková O, Pelouch V, Novák F. Phospholipid composition in the rat heart exposed to pressure overload from birth. Physiol Res 1996;45:83–5.
[28] Jezková J, Nováková O, Kolár F, Tvrzická E, Neckár J, Novák F. Chronic hypoxia alters fatty acid composition of phospholipids in right and left ventricular myocardium. Mol Cell Biochem 2002;232:49–56.
[29] Saini-Chohan HK, Holmes MG, Chicco AJ, Taylor WA, Moore RL, McCune SA, et al. Cardiolipin biosynthesis and remodeling enzymes are altered during development of heart failure. J Lipid Res 2009;50:1600–8.
[30] Oka T, Lam VH, Zhang L, Keung W, Cadete VJ, Samokhvalov V, et al. Cardiac hypertrophy in the newborn delays the

maturation of fatty acid beta-oxidation and compromises postischemic functional recovery. Am J Physiol Heart Circ Physiol 2012;302:H1784–94.
[31] Katragadda D, Batchu SN, Cho WJ, Chaudhary KR, Falck JR, Seubert JM. Epoxyeicosatrienoic acids limit damage to mitochondrial function following stress in cardiac cells. J Mol Cell Cardiol 2009;46:867–75.
[32] van Dijk A, Vermond RA, Krijnen PA, Juffermans LJ, Hahn NE, Makker SP, et al. Intravenous clusterin administration reduces myocardial infarct size in rats. Eur J Clin Invest 2010;40:893–902.
[33] Oliva J, French SW, Li J, Bardag-Gorce F. Proteasome inhibitor treatment reduced fatty acid, triacylglycerol and cholesterol synthesis. Exp Mol Pathol 2012;93:26–34.
[34] Yamashita H, Bharadwaj KG, Ikeda S, Park TS, Goldberg IJ. Cardiac metabolic compensation to hypertension requires lipoprotein lipase. Am J Physiol Endocrinol Metab 2008;295: E705–13.
[35] Alger HM, Brown JM, Sawyer JK, Kelley KL, Shah R, Wilson MD, et al. Inhibition of acyl-coenzyme A: cholesterol acyltransferase 2 (ACAT2) prevents dietary cholesterol-associated steatosis by enhancing hepatic triglyceride mobilization. J Biol Chem 2010;285:14267–74.
[36] Fassot C, Briet M, Rostagno P, Barbry P, Perret C, Laude D, et al. Accelerated arterial stiffening and gene expression profile of the aorta in patients with coronary artery disease. J Hypertens 2008;26:747–57.
[37] Boheler KR, Volkova M, Morrell C, Garg R, Zhu Y, Margulies K, et al. Sex- and age-dependent human transcriptome variability: implications for chronic heart failure. Proc Natl Acad Sci U S A 2003;100(5):2754–9.
[38] Waehre A, Vistnes M, Sjaastad I, Nygård S, Husberg C, Lunde IG, et al. Chemokines regulate small leucine-rich proteoglycans in the extracellular matrix of the pressure-overloaded right ventricle. J Appl Physiol 2012;112: 1372–82.
[39] Hwang JJ, Allen PD, Tseng GC, Lam CW, Fananapazir L, Dzau VJ, et al. Microarray gene expression profiles in dilated and hypertrophic cardiomyopathic end-stage heart failure. Physiol Genomics 2002;10:31–44.
[40] Albig AR, Roy TG, Becenti DJ, Schiemann WP. Transcriptome analysis of endothelial cell gene expression induced by growth on matrigel matrices: identification and characterization of MAGP-2 and lumican as novel regulators of angiogenesis. Angiogenesis 2007;10:197–216.
[41] Nikolova A, Ablasser K, Wyler von Ballmoos MC, Poutias D, Kaza E, McGowan FX, et al. Endogenous angiogenesis inhibitors prevent adaptive capillary growth in left ventricular pressure overload hypertrophy. Ann Thorac Surg 2012:1509–17.
[42] Gabrielsen A, Lawler PR, Yongzhong W, Steinbrüchel D, Blagoja D, Paulsson-Berne G, et al. Gene expression signals involved in ischemic injury, extracellular matrix composition and fibrosis defined by global mRNA profiling of the human left ventricular myocardium. J Mol Cell Cardiol 2007;42: 870–83.
[43] Hellman U, Mörner S, Engström-Laurent A, Samuel JL, Waldenström A. Temporal correlation between transcriptional changes and increased synthesis of hyaluronan in experimental cardiac hypertrophy. Genomics 2010;96:73–81.
[44] Kern CB, Norris RA, Thompson RP, Argraves WS, Fairey SE, Reyes L, et al. Versican proteolysis mediates myocardial regression during outflow tract development. Dev Dyn 2007;236:671–83.
[45] Reddy S, Osorio JC, Duque AM, Kaufman BD, Phillips AB, Chen JM, et al. Failure of right ventricular adaptation in children with Tetralogy of Fallot. Circulation 2006;114:I37–42.
[46] Zheng J, Chen Y, Pat B, Dell'italia LA, Tillson M, Dillon AR, et al. Microarray identifies extensive downregulation of noncollagen extracellular matrix and profibrotic growth factor genes in chronic isolated mitral regurgitation in the dog. Circulation 2009;119:2086–95.
[47] Schott P, Singer SS, Kögler H, Neddermeier D, Leineweber K, Brodde OE, et al. Pressure overload and neurohumoral activation differentially affect the myocardial proteome. Proteomics 2005;5:1372–81.
[48] Faber MJ, Dalinghaus M, Lankhuizen IM, Bezstarosti K, Dekkers DH, Duncker DJ, et al. Proteomic changes in the pressure overloaded right ventricle after 6 weeks in young rats: correlations with the degree of hypertrophy. Proteomics 2005;5:2519–30.
[49] Sheikh AM, Barrett C, Villamizar N, Alzate O, Valente AM, Herlong JR, et al. Right ventricular hypertrophy with early dysfunction: a proteomics study in a neonatal model. J Thorac Cardiovasc Surg 2009;137:1146–53.
[50] Konstantinov IE, Coles JG, Boscarino C, Takahashi M, Goncalves J, Ritter J, et al. Gene expression profiles in children undergoing cardiac surgery for right heart obstructive lesions. J Thorac Cardiovasc Surg 2004;127:746–54.
[51] Sharma HS, Peters TH, Moorhouse MJ, van der Spek PJ, Bogers AJ. DNA microarray analysis for human congenital heart disease. Cell Biochem Biophys 2006;44:1–9.
[52] Ghorbel MT, Cherif M, Jenkins E, et al. Transcriptomic analysis of patients with Tetralogy of Fallot reveals the effect of chronic hypoxia on myocardial gene expression.J Thorac Cardiovasc Surg 2010;140:337–45 [e326].
[53] Mancini M, Petretto E, Kleinert C, Scavone A, De T, Cook S, et al. Mapping genetic determinants of coronary microvascular remodeling in the spontaneously hypertensive rat. Basic Res Cardiol 2013;108:316–20.